

# Geostrophic wind variability in the 50–60°N zone over Europe: the role of mid-troposphere atmospheric circulation macro-forms



Michał Marosz\* <sup>1a</sup>, Krzysztof Kożuchowski<sup>2</sup>

<sup>1</sup> University of Gdańsk, Poland

<sup>2</sup> Professor Emeritus, Poland

\* Correspondence: University of Gdańsk, Poland. E-mail: [m.marosz@ug.edu.pl](mailto:m.marosz@ug.edu.pl)

 <sup>a</sup> <https://orcid.org/0000-0002-4782-6569>

**Abstract.** Circulation in the mid-troposphere in moderate and high latitudes of the Northern Hemisphere can be characterised by the Vangenheim-Girs (VG) circulation macro-forms. The aim of the research was to analyse the VG macro-forms as a factor determining the general characteristics of the atmospheric circulation in mid-troposphere in the Euro-Atlantic region and low-troposphere air-flow characteristics in the profile (zonal belt) crossing Central Europe from Ireland to Kazan in Russia (5°30'W–44°00'E). Alongside the VG macro-form calendar, ERA-INTERIM data were used. The utilised meteorological variables comprised 500hPa geopotential height, SLP and air temperature at 995 sigma level. The temporal scope of the research was 35 years (1981–2015) and the resolution was 24h (12.00 UTC). The circulation in the low-troposphere was characterised by the geostrophic wind vector characteristics directly resulting from SLP and air temperature fields. Subsequently, derived indices (e.g. wind direction stability) were used. The presented results indicate that the variability of anemological conditions at SLP in the area of 50–60°N over Europe is in direct connection with the mid-troposphere circulation features. The differences are statistically significant across nearly the entire research area. This includes the reversal of the dominant air flow direction in some areas. The greatest variability in geostrophic wind characteristics due to W, E and C VG macro-forms is revealed in the central and eastern part of the 50–60°N zone – between the southern Baltic Sea and the western border of Russia.

**Key words:**  
 Vangenheim-Girs macro-forms,  
 geostrophic wind,  
 anemological conditions,  
 Europe

## Introduction

Mid-troposphere circulation in moderate and high latitudes of the Northern Hemisphere can be characterised in qualitative, simplified terms by the Vangenheim-Girs circulation types classification (a.k.a. VG macro-forms) (Vangenheim 1946, 1952; Girs 1964, 1974, 1981).

Over the Atlantic-Eurasian sector, in the zone extending from Greenland to Eastern Siberia, the

above classification comprises three macro-forms: zonal (*W*) with the dominance of the latitudinal air flow from the west, and two meridional ones (*E* and *C*) with a varying location of ridges and troughs formed by long waves with relatively large amplitude in the mid-troposphere (Rossby waves). The characteristics of VG macro-forms, apart from the original works of its authors, appear in later publications (including Lamb 1972; Degirmendžić et al. 2000; Sepp 2005; Marsz 2012, 2013; Hoy et al. 2013; Kożuchowski and Degirmendžić 2018). Here,

we present a simplified image of the macro-forms: *W*, *E* and *C* (Fig. 1) from the classic work by Lamb (1972) alongside the composites of average values of the 500 hPa isobaric surface height (HGT500) on the seasonal basis for the period 1981–2015. The 500hPa geopotential height field observed on particular days usually differs significantly (depending on the VG macro-form) from the generalised HGT500 surface patterns which serve as a reference in VG macro-form classification.

Wibig (1999a, b) used rotated PCA (Principal Component Analysis) and identified six circulation types at the 500hPa isobaric surface field over Europe and the North Atlantic: NAO type (corresponding to zonal circulation over the majority of the analysed area and concordant with the VG *W* macro-form), Scandinavian, Eastern European, East Atlantic, Mediterranean (the meridional circulation types) and blockade (with a high-pressure system over Great Britain, Denmark and Central Europe). Huth (2001) used a similar method and distin-

guished 12 circulation types at 500 hPa in winter and 13 in summer. Some of those types resemble the macro-forms identified in the VG classification. This applies mostly to *W* and *C* macro-forms. Marosz (2012) used Artificial Neural Networks and identified as many as 25 types of 500 hPa geopotential field types over Europe, which represent three basic classes of mid-troposphere circulation: zonal, wave and blockade. This division corresponds only partially to the VG circulation macro-forms.

It is worth noting that VG macro-forms, or, more precisely, the frequencies of their occurrence, show a statistically significant relationship with known circulation indices in the hemispheric scale (Barnston and Livezey 1987). The frequency of VG macro-form *W* positively correlates with the Arctic Oscillation (AO) and North Atlantic Oscillation (NAO), the frequency of the *E* macro-form correlates significantly with the Scandinavian pattern (SCAN), and the frequency of the *C* macro-form – with the East Atlantic-West Russia pattern (EA/

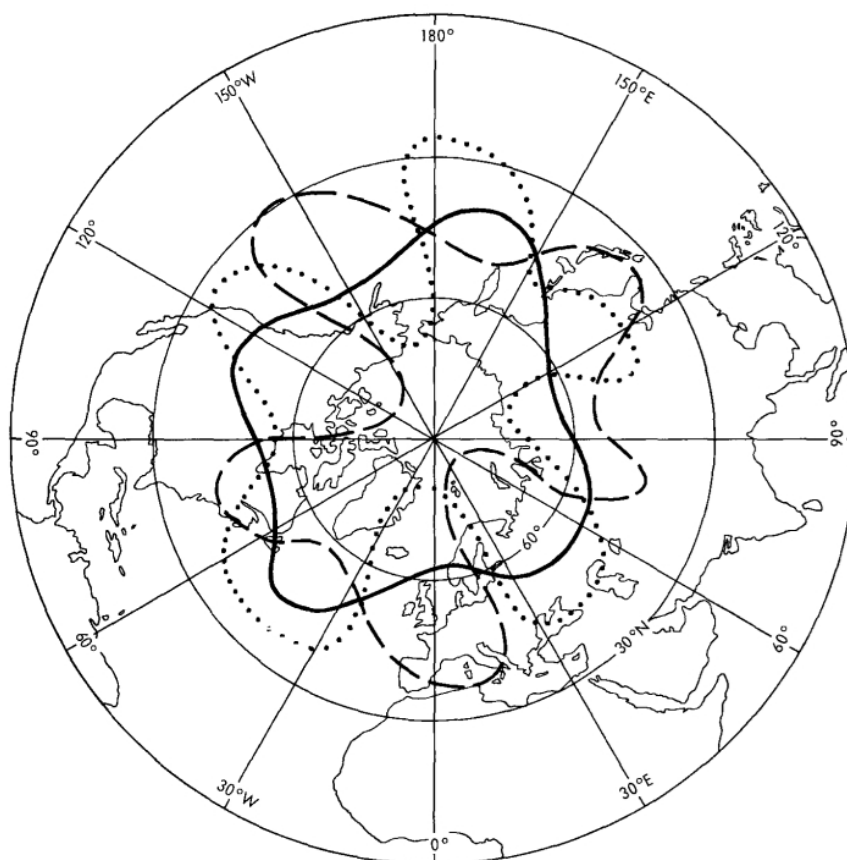


Fig. 1. Idealised 500 hPa contour defining the Vangenheim-Girs macro-forms (*W* – solid line, *C* – dotted line, and *E* – dashed line) over the Northern Hemisphere (after Lamb 1972)

WR). There is also a high correlation between the occurrence of the *W* macro-form and the depression rate of the Icelandic Low (Table 1). Therefore, it can be concluded that VG macro-forms *W*, *E* or *C* may be referred to as generalised patterns of mid-troposphere circulation, with the simultaneous assumption that their occurrence is not without connection with SLP (Sea Level Pressure) patterns.

In this paper we argue that VG macro-forms can be treated as factors shaping the SLP field and as such determine the anemological conditions of the lower troposphere in the profile crossing Central Europe from Ireland to Kazan in Russia (5°30'W–44°00'E) (Fig. 2). This profile approximately comprises the section of the 50–60°N zone in which the trough/ridge axes of Rossby waves are located. Their position defines the type of meridional circulation, i.e. VG macro-forms *E* or *C*, in the European sector. Its western part is occupied by the axis of the upper ridge of VG macro-form *C* or the axis of the trough in the case of macro-form *E*. On the other hand, in the eastern end of the analysed zonal belt lies the axis of a trough or a ridge (macro-forms *C* and *E*, respectively).

At the same time, the 50–60°N zone is a characteristic penetration route of the Atlantic air masses into the continent. This also applies to low-pressure systems tracks. Along the zone 50–60°N, 20–22 extratropical cyclones a year are moving eastward (Sepp 2005; Sepp et al. 2005). Bielec-Bąkows-

ka (2010) reports that over 37% of all European low-pressure systems occur in this zone. According to the classic classification of extratropical cyclones routes by van Bebber (1891), routes II, III and IVa and IVb occur within the zone 50–60°N that is the main route of cyclones' paths over the European continent. It can be stated that the zone extending from Ireland and Scotland through Denmark and the Baltic Sea towards the east is a characteristic area of atmospheric circulation activity in Europe.

Geostrophic wind vector is a synthetic and useful measure of variability of atmospheric circulation (and more generally anemological conditions) widely used in climatological research, especially when the available data cannot be considered homogeneous (WASA 1998). It was also utilised: in the classification of circulation types (Lityński 1969); in the study of trends in changes of circulation conditions (Kożuchowski 2004; Marosz 2016, 2017; Nowosad 2017); and in the assessment of its impact on other climate elements (Degirmendžić et al. 2004). It was also used in *downscaling* procedures and country regionalisation based on the variability of geostrophic wind characteristics (Miętus 1993, 1995; Marosz and Miętus 2012). In our study, the geostrophic wind vector serves as a synthetic description of the air flow in the lower atmosphere over Europe in the 50–60°N zone. The geostrophic wind vector is based on the horizontal gradient of sea-level pressure (SLP). Its characteristics' variability is investi-

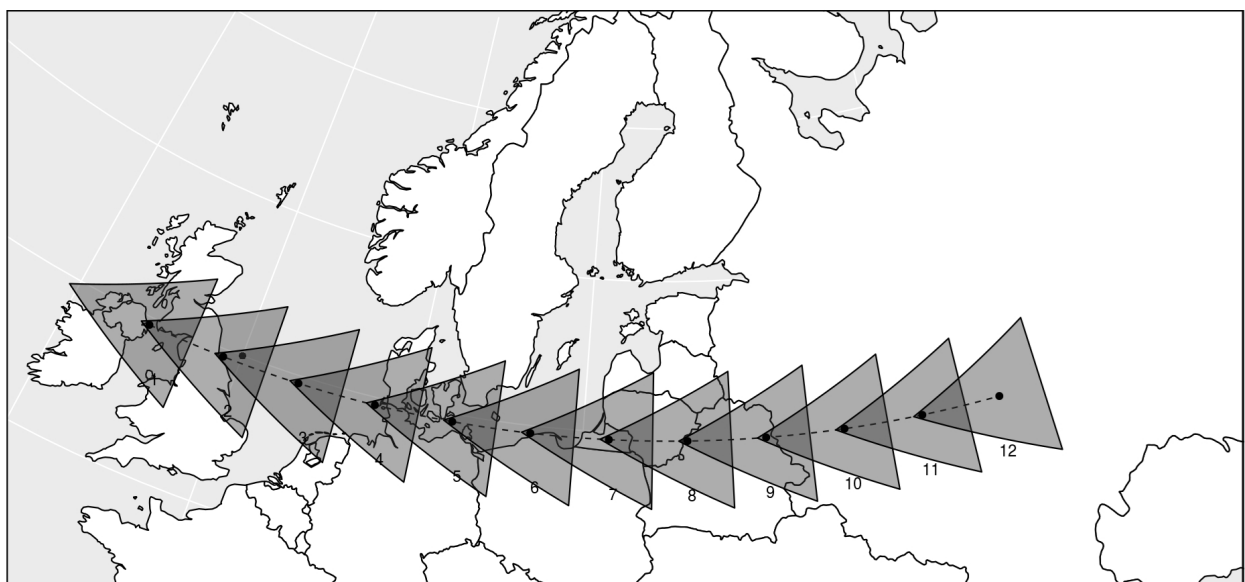


Fig. 2. Research area (50–60°N zone) – location of triangles (1 to 12) and points (back dots) at which geostrophic wind characteristics have been calculated

gated here as a potential response of near surface airflow to circulation conditions prevailing in the mid-troposphere (i.e. VG macro-forms).

The SLP field varies in direct relation to long waves' location in the mid-troposphere, according to well-known rules stating that the low-troposphere high-pressure systems occur at the eastern edges of the upper ridge, and the low-pressure systems tend to form on the western side of those ridges (Fig. 1 in Marsz 2013). In general, the correlation between SLP and the Vangenheim-Girs circulation macro-forms confirms those regularities (Sepp and Jaagus 2002; Sepp 2005; Marsz 2013). Kożuchowski and Degirmendžić (2018) have shown that the VG macro-forms are significant factors in shaping the circulation in the lower atmosphere over the North Atlantic and European areas. The macro-form *W* corresponds to a substantial negative SLP anomaly in the zone of high latitudes over Europe. During the occurrence of macro-form *E*, high-pressure systems develop in north-eastern Europe taking the form of a pronounced ridge of the Asian High in winter. During episodes of macro-form *C*, a high-pressure system occurs over Western Europe. In summer it is in the form of an Azores High ridge.

It should be emphasised that the pressure systems and their location specified above were determined on the basis of mean SLP values. The average location of isobars can only approximate, sometimes with considerable deviations, the actual, day-to-day pressure system location and associated circulation conditions. Location of mid-troposphere long waves, as well as low-troposphere lows and highs may differ significantly from the aforementioned averaged contour lines (at 500 hPa) or isobars (SLP). Therefore, we recognise that, for a more complete and objective circulation characteristic in the lower troposphere and the determination of its relationship with macro-forms of the mid-troposphere circulation, another measure of airflow is needed. We use the features (components and module) of the geostrophic wind vector, which allow an analysis of the directional structure, as well as airflow intensity, in the selected profile over Europe.

This study determines the variability of the airflow across part of the European continent depending on the atmospheric circulation conditions in the mid-troposphere. We analyse the variability of geostrophic wind vector characteristics in the profile

(defined by the central points of the twelve triangles) extending through the 50–60°N zone (Fig. 2). The analysis investigates the aforementioned issues in a seasonal scope for the VG macro-forms' occurrences. The more general purpose of the work is to check the suitability of the VG types calendar for the characteristics of anemological relations prevailing in the lower atmosphere over the selected area.

## Data and methods

The used data comprise a calendar of VG macro-forms, geopotential height of 500 hPa isobaric surface (HGT500), Sea Level Pressure (SLP) and air temperature at *sigma*995 level (i.e. near the surface). The temporal scope of the analysis covered 35 years (1981–2015) and resulted from the availability of data in the ERA-Interim reanalysis (Dee et al. 2011) nowadays considered to be the one of the state-of-the-art databases allowing analysis of climate variability.

The basis for this study is the calendar of occurrence of VG macro-forms extending from 1 January 1981 to 31 December 2015 (35 years). Data from the period 1981–2005 came from the publication by Dimitriev and Belyazo (2006), while data from the decade of 2006–2015 were prepared in the Arctic and Antarctic Research Institute in St. Petersburg and were retrieved thanks to the kind help of Professor A.A. Marsz. Unfortunately, in this 10-year series, there is a missing data period: April–September 2006 (183 days). In total, the mid-troposphere VG atmospheric circulation types calendar comprised over 12,000 days.

From the very methodological assumptions of the VG macro-forms identification, the flow of air in mid-troposphere will be significantly diversified in individual types. The features of the flow determined in this study based on the spatial variability in the geopotential height of the 500hPa isobaric surface (HGT500). The data were obtained from the ERA-Interim Reanalysis (Dee et al. 2011). The spatial resolution of the data was 0.75° by 0.75° longitude/latitude, while temporal resolution was 24h (12:00 UTC). The spatial range included the broadly defined Atlantic-European area (40°W–80°E, 35–75°N).

For the analysis of lower troposphere airflow, SLP data were used. Spatial resolution and time span are identical with the 500hPa geopotential data (i.e., ERA – INTERIM). The spatial scope of the SLP field for the analysis of airflow characteristics at sea level covered a zonal belt between 50–60°N and 10°W–50°E. Sea Level Pressure at the vertices of triangles (Fig. 2) and the interpolated value of the air temperature (at *sigma995* level) at the point of origin of the vector (the centre of gravity of the triangle) were used to calculate the components ( $u$ ,  $v$ ) and the module ( $V_{vel}$ ) of geostrophic wind vector. Geostrophic wind is defined as a theoretical airflow, assuming no friction and balance between the horizontal pressure gradient force and Coriolis force. A detailed description of the geostrophic flow assumptions is beyond the scope of this article, but it is comprehensively discussed in most meteorology and climatology textbooks. The details of the method of calculating the geostrophic wind vector based on SLP values (in triangles' vertices) with an adjustment for air temperature (hence air density) are presented in Miętus (1996), Marosz and Miętus (2012) and Marosz (2016, 2017).

The general formula for the geostrophic wind speed can be presented as follows:

$$\vec{V}[ms^{-1}] = \frac{1}{2\rho\omega\sin\phi} \cdot \nabla p \quad (1)$$

where:

$V$  – geostrophic wind speed,

$\omega$  – the angular velocity of the Earth,

$\Phi$  – latitude,

$\rho$  – air density at *sigma995* level,

$\nabla p$  – horizontal pressure gradient.

It allows the characteristics of geostrophic wind vector to be calculated:  $u$  (zonal component),  $v$  (meridional component),  $\alpha$  (azimuth – wind direction), and  $V_{vel}$  (velocity – vector module). In this analysis, using above variables, we calculated (in seasonal scale) additional characteristics: the resulting (vector sum) of the wind speed –  $V_g = (u^2 + v^2)^{0.5}$ , the mean geostrophic wind direction –  $V_g\alpha$ , the coefficient of stability of the wind direction –  $\eta$  (being a ratio of  $V_g$  and average of  $V_{vel}$ ), and the frequency of geostrophic wind directions –  $fV_g$  (in the classical 16-direction scheme). Analysis of those characteristics, corresponding to the occurrence of the VG circulation macro-form, allowed varying geostroph-

ic flow characteristics in the 50–60°N zone to be analysed.

Additional synthetic indices determining the impact of the VG circulation macro-forms on geostrophic wind characteristics were also calculated. For geostrophic wind parameters ( $V_g$ ,  $V_{vel}$ ) for each triangle, differences between the circulation macro-forms ( $W$ ,  $E$ ,  $C$ ) were calculated:

$$\begin{aligned} \Delta V_1 &= |V(W) - V(E)| \\ \Delta V_2 &= |V(W) - V(C)| \\ \Delta V_3 &= |V(E) - V(C)| \end{aligned} \quad (2)$$

where:

$V$  – selected parameter, e.g.  $V_g$ .

Averages ( $\Delta_3 V$ ) of those differences in the 12 points of the 50–60°N zone (Fig. 2) were subsequently analysed.

$$\Delta_3 V = (\Delta V_1 + \Delta V_2 + \Delta V_3) / 3 \quad (3)$$

The values of those statistics (indices based on three differences) reflect the overall effect of VG macro-forms on geostrophic wind characteristics.

In the case of differences in the resulting geostrophic wind velocity  $\Delta_3 V_g$ , an indicator ( $\Delta_3 V_g \alpha$ ) was additionally calculated. It shows how much of the difference  $\Delta_3 V_g$  depends on the variation of the  $\alpha V_g$  directions:

$$\Delta_3 V_g \alpha = (\Delta_3 V_g - \Delta_3 V_{vel}) / \Delta_3 V_g. \quad (4)$$

Values of differences between  $V_g$  vectors have a limitation, resulting from the highest geostrophic wind velocity associated with a specific circulation type. The sum of the three differences in the speed vector modules cannot exceed the doubled value of the highest module value. Therefore, the indicator ( $\Delta_3 V_g \beta$ ) was analysed. This determines the value of  $\Delta_3 V_g$  in relation to the largest of the three velocity modules  $V_{vel}(W)$ ,  $V_{vel}(E)$ ,  $V_{vel}(C)$ , corresponding to the individual circulation macro-forms

$$\Delta_3 V_g \beta = \Delta_3 V_g / \max(V_{vel}). \quad (5)$$

When comparing the frequency distributions of wind direction ( $fV_g$ ), the mean square frequency differences ( $\Delta fV_g$ )<sup>2</sup> were calculated for the 16-direction wind rose. The differences were compared with

the average expected frequency in the uniform distribution (i.e.  $f_{ave}=6.25\%$ ). The index of variation of three distribution of directions frequency was calculated as:

$$\Delta_3 V_g f = [^{1/}_{16} \Sigma(\Delta_3 f V_g)^2]^{0.5} / f_{ave} \quad (6)$$

Additionally, the distributions of geostrophic wind vector characteristics ( $u, v, V_{vel}$ ) were tested for the differences in their empirical cumulative distributions via the non-parametric Kolmogorov–Smirnov test. All triangles (12) and all possible combinations between VG macro-forms (3) were tested in the seasonal scope, yielding 144 instances.

The procedure followed the classical Kolmogorov–Smirnov testing scheme, which identifies the maximum difference ( $D_s$ ) between empirical cumulative distributions ( $F_n$  and  $F_m$ ) of two variables  $x_1$  and  $x_2$  (Wilks 2011) and subsequently compares it with a critical value from a Kolmogorov–Smirnov distribution with a no-difference statement serving as a null hypothesis.  $D_s$  equals:

$$D_s = \max_x |F_n(x_1) - F_m(x_2)|, \quad (7)$$

## Results

### Occurrence of the VG macro-forms

In the analysed period (1981–2015), the VG macro-form *E* had the highest frequency ( $f_d$ ) – on the average 43.5% of days a year (i.e.,  $f_d=159$  days/year) and reached its maximum of over 70% of days in 1981 (262 days). The circulation type *W* occurred on average in 33.4% of days, and *C* type – in 23.1% ( $f_d=122.0$  and  $f_d=84.3$  days/year, respectively, Table 2).

Annual relations between the frequency of circulation forms (i.e.,  $f_d E > f_d W > f_d C$ ) are characteristic for all seasons except winter, when the frequency of the VG macro-form *W* reaches the highest value (37.2 days/season, i.e., 41.2% of days, Table 2). The participation of the circulation type *E* increases to over 50% in summer, whereas the frequency of the VG macro-form *C* rises to over 25% of the days in spring. The lowest  $f_d$  frequencies of macro-form *W*

occur in summer, macro-form *E* in winter and macro-form *C* in the fall.

In the multi-annual perspective, the annual frequency of the three forms of circulation is characterised by a high variability with variability coefficients (*V*) at 19–20%. The variation in occurrence frequency ( $f_d$ ) generally increases in winter. For the VG macro-form *E*, *V* is close to 50% and fluctuations in the frequency range from 0% (1991/92) to more than 60% (1984/85) days in a season. The variability in the frequency of the VG macro-form *W* is the most stable in spring (*V* = 18%, Table 2).

During the year there were, on average, 53.7 macro-form episodes, i.e. the number of consecutive days with the same VG macro-form, which refers to a “similar synoptic process” – a term introduced by Girs (1974). This means that the VG macro-forms changed on average every 6.8 days – approximately once a week. The number of episodes with macro-forms *W* and *E* was slightly higher (18.9) than the annual number of the episodes with the VG macro-form *C* (15.9, Table 2).

The total number of episodes of all macro-forms  $f_e (W + E + C)$  varied in the analysed period from 35 in 1984 to 69 in 2008. The number of episodes of the circulation type *W* exhibits the greatest variability – ranging from  $f_e=8$  in 1984 to  $f_e=30$  in 2008. The longest episodes (the VG macro-form *E*) have average duration of  $T=8.4$  days, with exceptionally long-lasting episodes of this form: 24 April – 17 August 1981 ( $T=116$  days), 21 January – 12 March 1984 ( $T=48$  days) and 17 June – 6 August 1988 ( $T=51$  days). The episodes with the macro-form

Table 1. Seasonal (DJFM) correlation coefficients of the VG macro-forms’ frequencies with selected circulation indices and SLP over SW Island, 1951–2017. Significant values ( $\alpha=0.05$ ) have been bolded

Circulation index	VG macro-forms		
	W	E	C
AO	<b>0.68</b>	<b>-0.40</b>	-0.01
NAO	<b>0.61</b>	<b>-0.38</b>	<b>-0.33</b>
SCAN	<b>-0.69</b>	<b>0.71</b>	-0.13
EA/WR	<b>0.33</b>	<b>-0.55</b>	<b>0.48</b>
SLP Island.	<b>-0.64</b>	<b>0.29</b>	<b>0.29</b>

Source of data: Standardized Northern Hemisphere Teleconnection Indices (1981–2010 Clim) [ftp://ftp.cpc.ncep.noaa.gov/wd52dg/data/indices/tele\\_index.nh](ftp://ftp.cpc.ncep.noaa.gov/wd52dg/data/indices/tele_index.nh)

*W* lasted 6.4 days on average, with the maximum of 29 days during 10 October – 7 November 1998. Macro-form *C* episodes lasted on average 5.3 days. In winter 1996/97 a 24-day episode occurred (16 December 1996 – 8 January 1997). Maxima of the average annual duration of the circulation types episodes equalled 15.3 (*E* macro-form episodes in 1984), 9.3 (*W* macro-form in 2002.) and 8.4 (*C* macro-form in 1997, Table 2).

### VG macro-forms versus HGT500 over Europe and SLP in the 50–60°N zone

Each of the VG macro-forms corresponds to a specific shape of HGT500 and the associated SLP fields. Figures 3 and 4 show composites (averages) of 500 hPa isobaric surface height (Fig. 3) and SLP (Fig. 4) during VG macro-forms: *W*, *E*, and *C*. Winter (DJF) and spring (MAM) spatial variability of SLP

and HGT500 are typical examples of the substantial difference between the seasonal averages resulting from the occurrence of the VG circulation types. These are also cases in which the average HGT500 field strongly reflects the VG macro-form defining/master pattern. This compliance occurs primarily for *W* and *C* types, while the averaged HGT500 values associated with *E* type show the typical mid-troposphere wave only in spring and to some extent also in summer.

In winter (DJF, Figs 3 and 4) HGT500 and SLP perfectly illustrate the zonal nature of atmospheric circulation during the occurrence of the VG macro-form *W*. Contour lines and isobars have a clear latitudinal course; meridional gradients are high and evenly distributed. Strong westerly zonal circulation occurs in both the mid- and lower troposphere.

In spring, the circulation type *E* forms a not-too-clearly marked wave in the HGT500 field com-

Table 2. Average (mean), maximum (max), minimum (min), standard deviation (sd) and variability coefficient (V) of seasonal (DJF – winter, MAM – spring, JJA – summer, SON – fall) and annual VG macro-form frequencies ( $f_d$  – days/year), number ( $f_c$ ) and average duration in days (T) (1981–2015)

VG	Measure	DJF fd	MAM fd	JJA fd	SON fd	YEAR (JAN–DEC)		
						fd	fc	T
W	mean	37.2	26.6	24.9	34.8	122.0	18.9	6.4
	max (year)	66 (1988/89)	41 (1994, 2000)	52 (2008)	53 (1986)	157 (2000)	30 (2008)	9.3 (2002)
	min (year)	8 (1995/96)	3 (1984)	4 (1981)	16 (1985)	58 (1981)	8 (1984)	4.5 (1981)
	sd	13.5	4.7	9.4	9.9	24.7	3.9	1.4
	V	0.36	0.18	0.38	0.29	0.20	0.21	0.22
	E	mean	31.1	43.0	46.5	37.5	159.0	18.9
max (year)		61 (1984/85)	70 (1983)	84 (1981)	60 (2000)	262 (1981)	24 (1982, 1999, 2014)	15.3 (1984)
min (year)		0 (1991/92)	11 (1997)	21 (2008)	19 (1995)	106 (1997)	12 (1997)	5.7 (2008)
sd		15.3	13.2	10.6	11.0	30.6	3.2	2.6
V		0.49	0.31	0.23	0.29	0.19	0.17	0.31
C		mean	22.1	23.4	20.7	18.7	84.3	15.9
	max (year)	45 (1991/92)	46 (1997)	36 (1995)	32 (1995)	118 (1997)	22 (1995)	8.4 (1997)
	min (year)	10 (1988/89)	8 (1986)	4 (1981)	0 (1984)	45 (1981)	8 (1981)	3.5 (1986)
	sd	8.6	8.8	7.6	7.0	15.7	2.8	1.5
	V	0.39	0.38	0.37	0.37	0.19	0.17	0.28

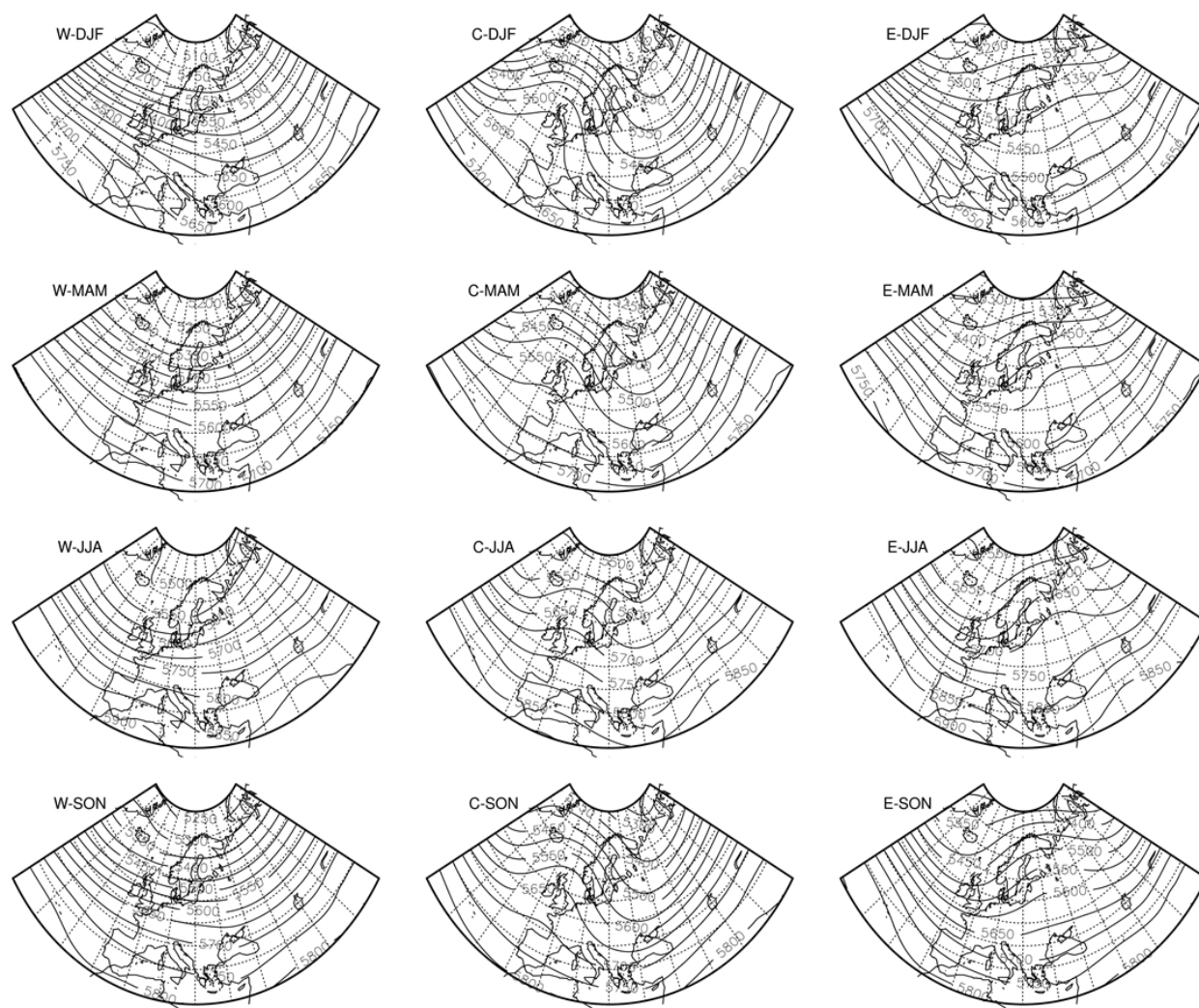


Fig. 3. Average seasonal HGT500 (gpm) during VG macro-forms' occurrence (1981–2015)

prising a trough over the North Atlantic and British Isles and a ridge over the eastern borders of Europe (Fig. 3). Sea Level Pressure in the 50–60°N zone over Europe is characterised by a pressure increasing from west to east. Gradients of HGT500, and SLP gradients during the dominance of the VG macro-form *E* are substantially smaller in comparison with those observed in zonal circulation type *W*. Sea Level Pressure isobars indicate the dominance of the southern circulation in the analysed zone (Fig. 4).

The HGT500 contour lines and SLP isobars associated with the dominance of *C* type (MAM, Figs 3 and 4) show an inverted circulation system compared to the *E* type, with the mid-troposphere wave being more clearly indicated. The ridge at 500 hPa stretches along an axis running through Ireland and Iceland, whereas the trough lies over Eastern Eu-

rope. In the 50–60°N zone over Europe, air pressure decreases to the east – the highest mean SLP values form the high-pressure system located over the North Sea off the coast of Scotland, i.e. in the eastern part of the mid-troposphere ridge. Horizontal pressure gradients in this zone reach their maximum between 20°E and 30°E, over the Baltic Sea and in Central-Eastern Europe, and are clearly higher than during the dominance of the VG macro-form *E* thus demonstrating the dominance of the advection from the north.

The SLP field in the 50–60°N zone associated with VG macro-forms varies significantly on a seasonal basis. In the warm season, the pressure gradients decrease and, in the case of the circulation type *E*, they also reverse the direction. During the domination of the *E* type, the influences of seasonal atmospheric circulation centres in the lower at-

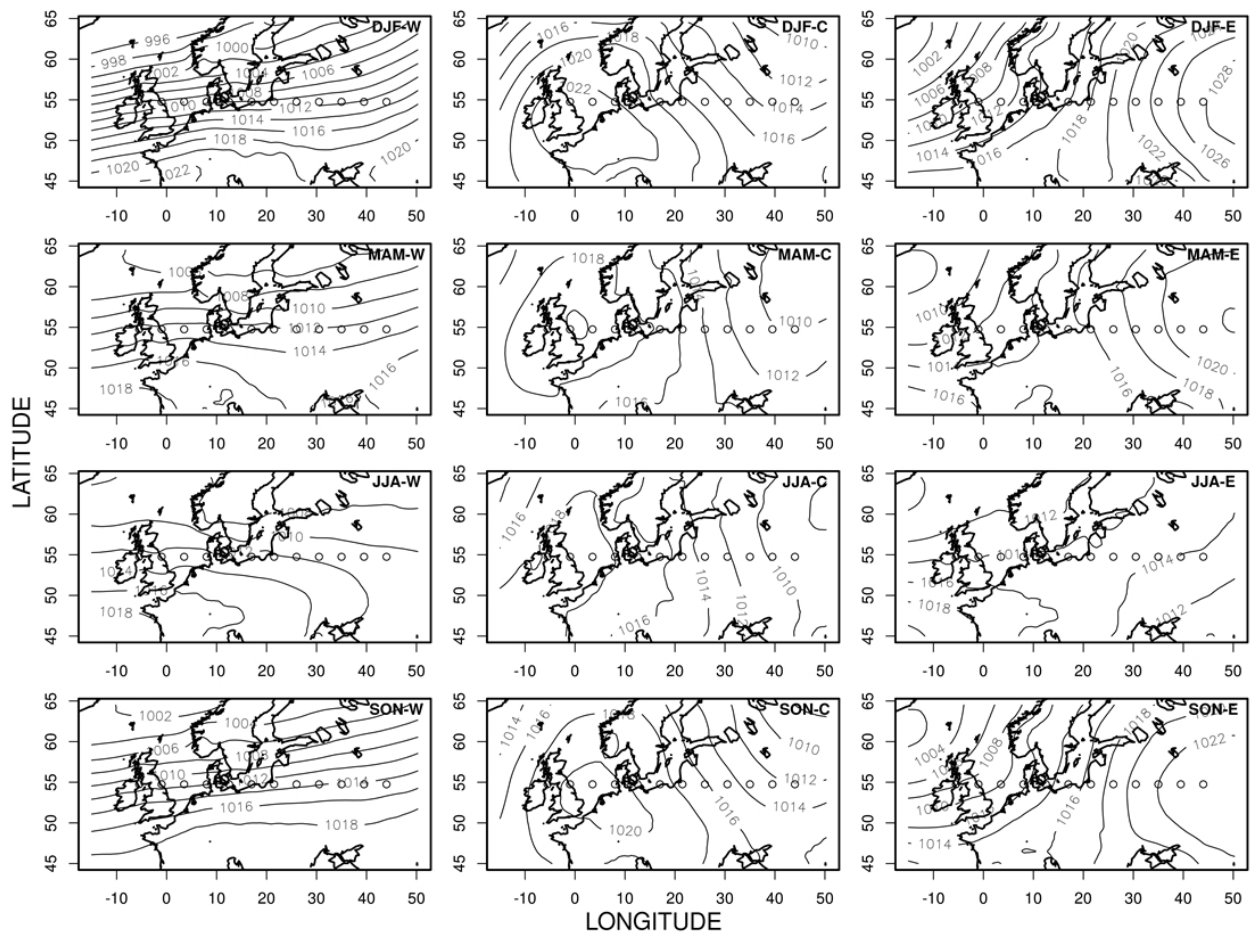


Fig. 4. Average seasonal SLP (hPa) during VG macro-forms' occurrence (1981–2015). Centres of triangles (1 to 12 – west to east) have been marked as white circles

mosphere become visible. In winter, the Asian High stretches west up to 20°E; in summer the pressure decreases slightly in the eastern and western part of the 50–60°N zone; however, weak-gradient areas dominate. During the dominance of the C type in all seasons, the presence of a blocking high-pressure system over the British Isles and the North Sea is characteristic; it is most clearly noticeable in winter.

**VG macro-forms versus the variability of geostrophic wind characteristics in the 50–60°N zone over Europe**

The average geostrophic wind velocities ( $V_{vel}$ ) reach the highest values during the domination of the VG macro-form W in winter. In the zone 50–60°N, the geostrophic wind associated with the W type gradually weakens towards the east: the average geostrophic wind velocity decreases from 16.1 ms<sup>-1</sup> at

the western end of the zone (triangle 1) to 11.4 ms<sup>-1</sup> at its eastern end (triangle 12). Average velocities ( $V_{vel}$ ) associated with other macro-forms are generally much smaller. Only in summer in the eastern part of the research area, C macro-form results in  $V_{vel}$  that is slightly higher than the speed associated with the macro-form W (7.1 and 6.2 ms<sup>-1</sup>, respectively). In summer both the  $V_{vel}$  absolute values and their variability in the zone 50–60°N decrease (Fig. 5 – panel V).

The zonal ( $u$ ) component of the geostrophic wind velocity in zone 50–60°N varies similarly to the geostrophic wind vector velocity. Its values are much lower (up to 11.4 ms<sup>-1</sup> during the occurrence of macro-form W). In some parts of the zone in the case of macro-forms E and C it is negative, indicating eastern advection (on average). The eastern component of the geostrophic wind appears most clearly in spring. In the case of the circulation macro-form E, it covers almost the entire zone (from

triangle 4 eastward). In summer the eastern advection comprises the easternmost part of the zone – triangles 8 to 12. Small negative values also appear in spring, with the occurrence of macro-form C in the western half of the 50–60°N zone.

The meridional component ( $v$ ) in the 50–60°N zone varies from  $4.9 \text{ ms}^{-1}$  (VG macro-form E, triangle 8, DJF) to  $-4.1 \text{ ms}^{-1}$  (VG macro-form C, triangle 8, MAM). It is characteristic that the absolute values of  $v$  increase significantly in the central and eastern part of the zone. For type E it is southern advection, and northern for C. It is worth noting that at the western end of the zone (triangles: 1, 2) the  $v$  component for the VG macro-form C changes sign and indicates southern advection. This also means that this part of the zone is located west of the SLP high-pressure centre over England and the North Sea (Fig. 4) and simultaneously near to the

ridge axis shaping the circulation type C (Fig. 5, panel:  $u, v$ ).

In seasonal scope the resultant vector ( $V_g$  – vector sum of  $u$  and  $v$ ) of the geostrophic wind is characterised by the vector azimuth (i.e. direction of  $V_g$ ), velocity value  $V_g = (u^2 + v^2)^{0.5}$  and a coefficient of wind direction stability  $\eta = V_g / \text{mean}(V_{vel})$ . Figure 5 presents the variability of dir and  $\eta$  values in zone 50–60°N, whereas Table 3 presents the resultant  $V_g$  values and azimuths presented in the 16-direction wind rose naming convention (22.5° segments).

The VG macro-form W corresponds, throughout the zone, to a slightly varying azimuth of  $V_g$  close to 270°, i.e. western advection (W, WNW and WSW directions). The value of  $V_g$  in the zone 50–60°N reaches  $11.4 \text{ ms}^{-1}$  in winter,  $6.4 \text{ ms}^{-1}$  in spring and summer and shows a decreasing tendency towards the east. However, in summer, and to some

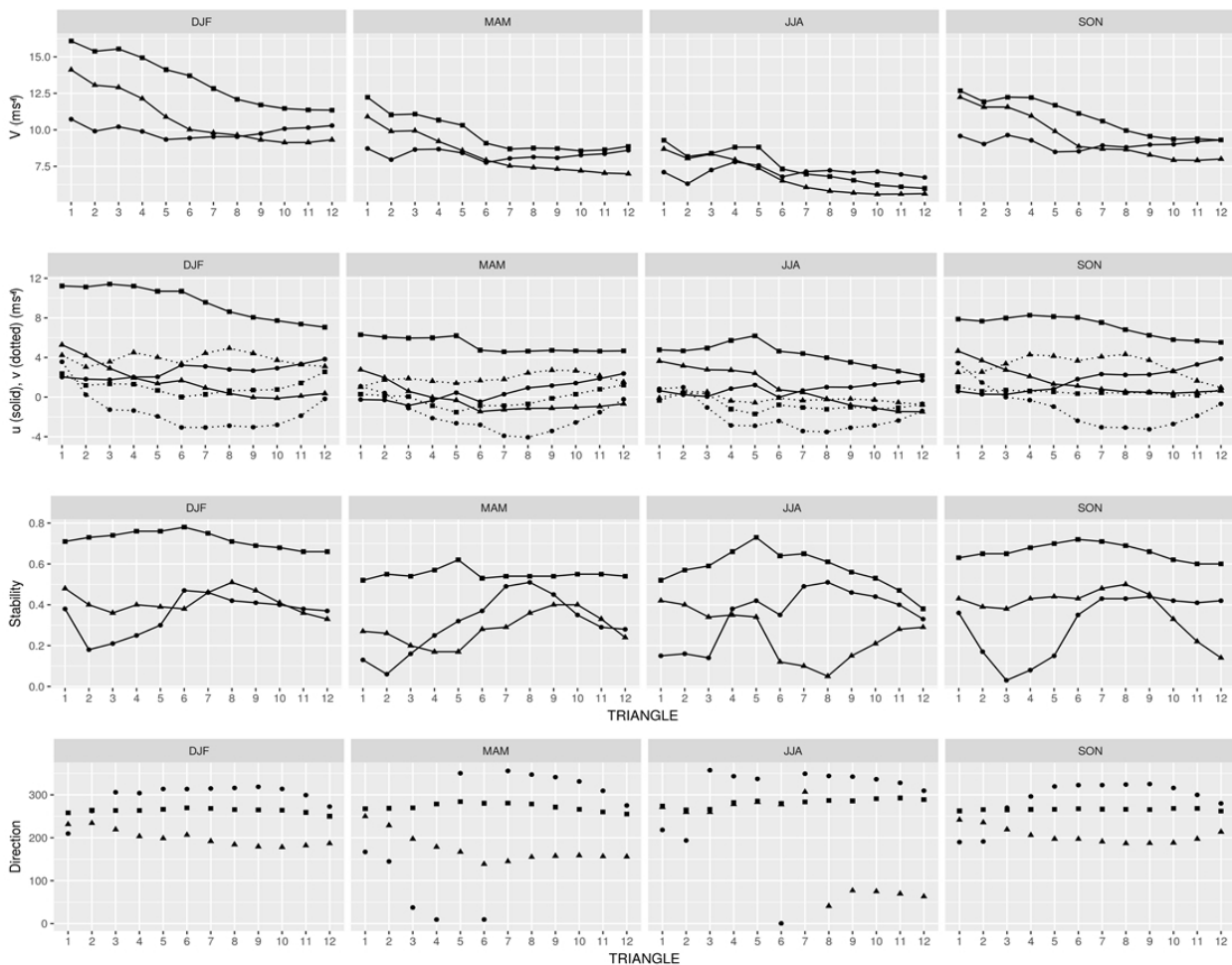


Fig. 5. Seasonal geostrophic wind characteristics at selected locations (triangles 1 to 12 – west to east) for the VG macro-forms: circle – C, triangle – E, square – W:  $V$  – velocity;  $u$  – zonal component,  $v$  – meridional component, stability – wind direction stability coefficient, direction – average wind direction, 1981–2015

**Table 3.** Averages of geostrophic wind directions and vector sum of wind speed  $V_g$  ( $\text{ms}^{-1}$ ) in the 50–60°N zone for triangles 1 to 12 (west to east). Triangles with maximum values of stability coefficient are bolded, 1981–2015

Triangle / Season	1	2	3	4	5	6	7	8	9	10	11	12
<b>VG macro-form W</b>												
DJF	WSW 11.4	W 11.2	W 11.5	W 11.4	W 10.7	<b>W</b> <b>10.7</b>	W 9.6	W 8.6	W 8.1	W 7.8	W 7.5	WSW 7.5
MAM	W 6.4	W 6.1	W 6.0	W 6.1	<b>WNW</b> <b>6.4</b>	W 4.8	W 4.7	W 4.7	W 4.7	W 4.7	W 4.8	WSW 4.8
JJA	W 4.8	W 4.7	W 5.0	W 5.8	<b>WNW</b> <b>6.4</b>	W 4.7	WNW 4.5	WNW 4.2	WNW 3.7	WNW 3.3	WNW 2.9	WNW 2.3
SON	W 8.0	W 7.8	W 8.0	W 8.3	W 8.2	<b>W</b> <b>8.0</b>	W 7.5	W 6.9	W 6.3	W 5.8	W 5.6	W 5.6
<b>VG macro-form E</b>												
DJF	SW 6.8	SW 5.2	SW 4.7	SSW 4.9	SSW 4.2	SSW 3.8	SSW 4.5	<b>S</b> <b>4.9</b>	S 4.4	S 3.7	S 3.3	S 3.1
MAM	WSW 2.9	SW 2.6	SSW 2.0	S 1.6	SSE 1.5	SE 2.2	SE 2.2	SSE 2.7	<b>SSE</b> <b>2.9</b>	<b>SSE</b> <b>2.9</b>	SSE 2.3	SSE 1.7
JJA	<b>W</b> <b>3.7</b>	W 3.2	W 2.8	W 2.8	WNW 2.5	W 0.8	NW 0.6	NE 0.3	ENE 0.9	ENE 1.2	ENE 1.6	ENE 1.6
SON	WSW 5.3	SW 4.5	SW 4.4	SSW 4.7	SSW 4.4	SSW 3.8	S 4.2	<b>S</b> <b>4.3</b>	S 3.7	S 2.6	SSW 1.7	SSW 1.1
<b>VG macro-form C</b>												
DJF	SSW 4.1	W 1.8	NW 2.1	NW 2.5	NW 2.8	<b>NW</b> <b>4.4</b>	NW 4.4	NW 4.0	NW 4.0	NW 4.0	WNW 3.9	W 3.8
MAM	SSE 1.1	SE 0.5	NE 1.4	N 2.2	N 2.7	N 2.8	N 3.9	<b>NNW</b> <b>4.2</b>	NNW 3.6	NNW 2.9	NW 2.4	W 2.4
JJA	SW 1.1	SSW 1.0	N 1.0	WNW 3.0	NNW 3.2	N 2.4	N 3.5	<b>NNW</b> <b>3.7</b>	NNW 3.3	NNW 3.1	NNW 2.8	NW 2.2
SON	S 3.5	S 1.5	W 0.3	WNW 0.7	NW 1.3	NW 3.0	NW 3.8	NW 3.8	<b>NW</b> <b>4.0</b>	NW 3.8	WNW 3.8	W 3.9

extent in fall,  $V_g$  maximum shifts towards the central part of the area and the strongest western air flow occurs over the North Sea, the Baltic Sea and Western Denmark (Table 3). Over the western and southern Baltic Sea (triangles: 5, 6), also in other seasons, the western winds associated with the VG

macro-form *W* have the highest stability. Wind direction stability coefficients reach values of  $\eta=0.63$  in spring and  $\eta=0.78$  in winter (triangle 5).

The resultant  $V_g$  values associated with the circulation type *E* rarely exceed  $5 \text{ ms}^{-1}$ . They are particularly low in summer, which confirms the prevailing

occurrence of the weak-gradient SLP field in zone 50–60°N (Fig. 4). Advection from the southern sector dominates. The  $V_g$  values from the directions S and SSE are relatively high, and in addition, those cases are characterised by fairly high overall directional stability. In winter the stability coefficient equals  $\eta=0.51$ . The most stable directions of geostrophic wind occur in the eastern part of zone 50–60°N (triangles: 8–10). In the western part of the zone, during the dominance of the VG macro-form *E*, there is an average air flow from the west and in the summer this is accompanied by a fairly high stability ( $\eta=0.42$ , triangle 1) and velocity  $V_g$  ( $3.7 \text{ ms}^{-1}$ ). Weak advection from the eastern sector appears in the eastern part of zone 50–60°N, starting from triangle 8, i.e. over Russia (Fig. 5).

The VG macro-form *C* results in north-western advection in most of the 50–60°N zone. Only in the western fringe of the zone are the geostrophic wind vector  $V_g$  directions S, SW and W (Table 3). The resultant  $V_g$  values show a significant upward trend in the eastward direction – their maxima appear in the area from the southern Baltic to the area of Smolensk (Russia) (triangles: 5–9). There too, the average direction of geostrophic wind vector shows NW and NNW advection and overall highest stability (in spring and summer  $\eta=0.51$ ).

### VG macro-forms versus CDFs of geostrophic wind characteristics

The Kolmogorov–Smirnov (KS) test confirms the existence of differences in geostrophic wind characteristics' CDFs (Cumulative Distribution Functions) due to the VG macro-forms. Over the majority of the research area and in most of the seasons the empirical cumulative distributions vary significantly (Table 4). In the case of the  $u$  (zonal) component, only three times (out of 36) were differences not significant, and all three of these cases refer to differences between *C*- and *E*-inducing circulation types. They occurred in MAM, JJA and SON (triangles: 4, 7, 5, respectively) indicating the area of south and western Baltic Sea and west of Denmark.

In winter for  $v$  (meridional component) in triangles 2 (*C* vs. *W*) and 12 (*W* vs. *E*) the differences prove to be insignificant. The spatial extent is more

concise in summer when western (triangles 1 to 3) and eastern (triangles 11, 12) boundaries of the research area seem not to be influenced by the VG macro-forms (*W* vs. *E*) with respect to near-surface meridional flow. In spring, for nearly all triangles (except triangle 2 – *C* vs. *W* macro-forms), there occurs a significant influence of the VG macro-forms on geostrophic wind meridional component. In fall only the easternmost triangle (12) does not exhibit significant differences, and this refers to *W*-vs.-*E*-type-induced differences.

More frequent events of no-difference (due to the VG macro-forms forcing) situations occur in the case of geostrophic wind velocity ( $V_{vel}$ ) cumulative distributions, but still those cases are not abundant. In winter, only triangles 8 and 9 (southern Baltic) do not exhibit significant differences (*C* vs. *E* macro-forms). In spring, this situation occurs for *C* vs. *E* macro-forms (triangles: 5 to 7) and *C* vs. *W* macro-forms (triangles, 8, 11, 12). In summer, triangles 4, 5, 6 (*C* vs. *E* macro-form) and 7 (*C* vs. *W* macro-form) do not vary, whereas in fall this applies to triangles 6 to 8 (*C* vs. *E* macro-form), 11, 12 (*C* vs. *W* macro-form) and 2 (*W* vs. *E* macro-form).

### Variability of directional structure of geostrophic wind

In the context of the wind directions, wind speed and directional stability, three characteristic sections manifest themselves in the analysed 50–60°N zone. Wind roses representing those sections (triangle 1 over Ireland, triangle 6 over southern Baltic and triangle 8 over Vitebsk region) illustrate the development of diversified anemological conditions in individual sectors of the 50–60°N zone depending on the VG circulation macro-forms (Fig. 6).

In the western part of the zone (Fig. 6, left panel) there is a dominance of the southern advection associated with the VG macro-form *C* and the prevalence of airflow from the western sector during the reign of the circulation type *E*. In the central part of the zone (Fig. 6, middle panel) the most stable and intense western flow stands out and is associated with the zonal circulation type *W*. Relatively high frequency of the NW direction is associated with meridional circulation *C*. The third section

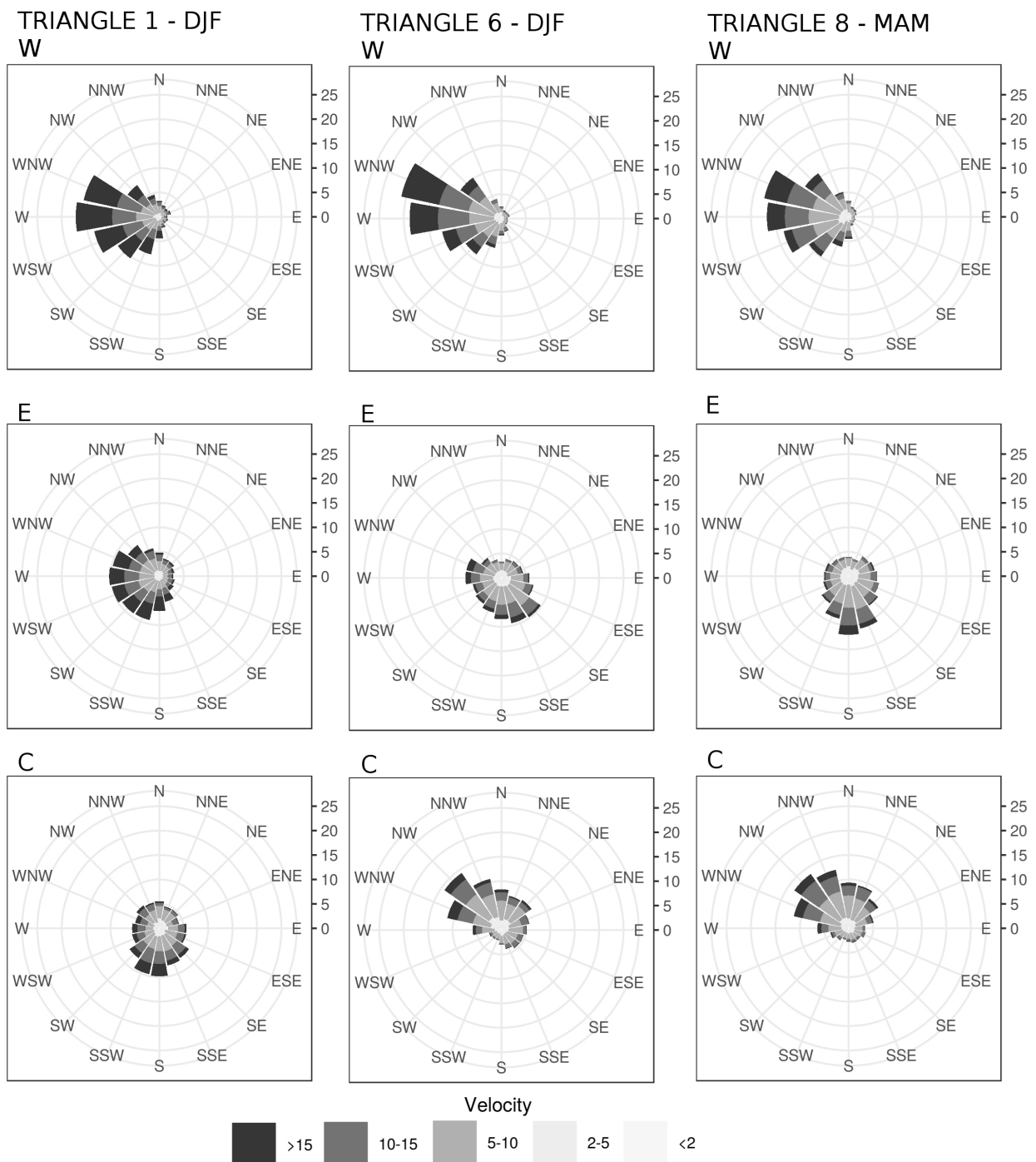


Fig. 6. Wind roses for selected triangles and seasons in VG macro-forms W, E and C, 1981–2015

(Fig. 6, right panel) covers the eastern part of the zone, with the pronounced dominance of the southern advection associated with the VG macro-form *E* in spring. Also, elevated frequencies of WNW, NW and NNW directions are maintained during the *C* circulation type.

The directional structure of geostrophic wind in the 50–60°N zone and its seasonal variability are

presented in Figure 7. The frequency of directions with the western component – SSW–NNW – prevails throughout the zone. This is most marked in winter, but also quite clear in summer, which corresponds to seasonal fluctuations in the intensity of zonal circulation in mid latitudes.

Geostrophic wind directions with the highest frequencies mostly correspond to the average di-

rection of the vector  $V_g$  (Table 3). Occasional differences do not exceed 1/16 of the full angle (i.e., one sector of the directional wind rose).

In summer, the WNW direction for the VG macro-form  $W$  reaches the overall maximum frequency (26.4%) (Fig. 7). Such frequency is nearly four times higher than the mean of 16 directions (6.25% is the expected value with a uniform distribution of directional frequency). In winter, the frequency of the  $W$  wind direction reaches 23.4%, in spring and fall – it is slightly above 21%. On the other hand in spring, during the dominance of the macro-form  $E$  the western directions (WSW,  $W$  or WNW) appear with a frequency as low as 2.8%, and 3–5% in the remaining seasons. Similar percentages of WSW–WNW direction frequencies occur during the dominance of the VG macro-form  $C$ .

The occurrence of the circulation macro-form  $E$  results with the highest frequencies of S wind directions (16.8% in fall and 15.7% in winter). The highest frequency (16%) of the NW direction in spring is associated with the macro-form  $C$ . Meridional circulation macro-form results in quite balanced directional structure. Also, directional stability is clearly lower than in the prevalence of westerly wind direction that is associated with the macro-form  $W$ . The mentioned values refer to various locations in the analysed zone (Fig. 7).

### VG macro-forms versus synthetic measures of $V_g$ variability

Differences between frequency distributions – directional wind roses – associated with circulation types are most pronounced in the central and eastern part of the 50–60°N zone, which correlates with the stability of geostrophic wind directions. At the same time, they indicate the section of the zone subject to the strongest influence of the mid-troposphere circulation types: between triangle 5 and triangle 9 (Western Baltic – Vitebsk) where coefficients of variability of frequency distributions  $\Delta_3 V_g f$  (equation 6) are the highest (Table 5).

Similar regularities result from the analysis of the variation in the geostrophic wind velocity vector. The largest variation takes place in the same section of the zone (triangles 5–9). The average of

the  $V_g$  differences in winter exceeds 7 ms<sup>-1</sup> in this section, 6 ms<sup>-1</sup> in fall, 5 ms<sup>-1</sup> in spring and 3 ms<sup>-1</sup> in summer. At the western and eastern margin of the zone, these differences are smaller and do not reach 3 ms<sup>-1</sup> in the summer.

The coefficient  $\Delta_3 V_g \alpha$  (Eq. 4) quantifying the part of  $V_g$  variability resulting from  $V_g$  direction variability (Table 6) shows that the significance of  $V_g$  direction increases in the transitional seasons and is highest in the central and eastern part of the analysed zone. Only at the western border of the zone is the variability of  $V_g$  governed mainly by geostrophic wind velocity  $V_{vel}$  (Table 4).

The geostrophic vector wind speed modules gradually decrease from west to east of the analysed 50–60°N zone (Fig. 5). The  $\Delta_3 V_g \beta$  index (Eq. 5) makes it possible to assess the differences in  $\Delta_3 V_g$  regardless of those changes and – we think – reflects the real scale of geostrophic wind variability in particular parts of the 50–60°N zone depending on mid-troposphere circulation form. The variability of the  $\Delta_3 V_g \beta$  index is shown in Figure 8. The variability of  $V_g$  vectors grows gradually from west to east, up to the central-eastern part of the zone. Maxima of  $\Delta_3 V_g \beta$  occur in triangles 8 and 9 (Vitebsk–Smolensk). In spring, they reach the value of 0.66. It can be concluded that in this part of the zone the variability of the geostrophic wind depends to the highest extent on the VG macro-forms. This is primarily determined by the difference between the wind characteristics associated with macro-forms  $E$  and  $C$ .

It is worth noting that the fragment of 50–60°N zone distinguished by the strongest variability in geostrophic wind resulting from the VG macro-forms (triangles 8–9) at the same time coincides with the clearest contrasts between the advection directions in the mid-troposphere during the occurrence of the macro-form  $E$  (advection from the southern sector in the eastern part of the trough) and macro-form  $C$  (advection from the northern sector in the eastern part of the mid-troposphere ridge, see Fig. 1). It can be assumed that this is a non-accidental coincidence, demonstrating the circulation connection between the lower and mid-troposphere.

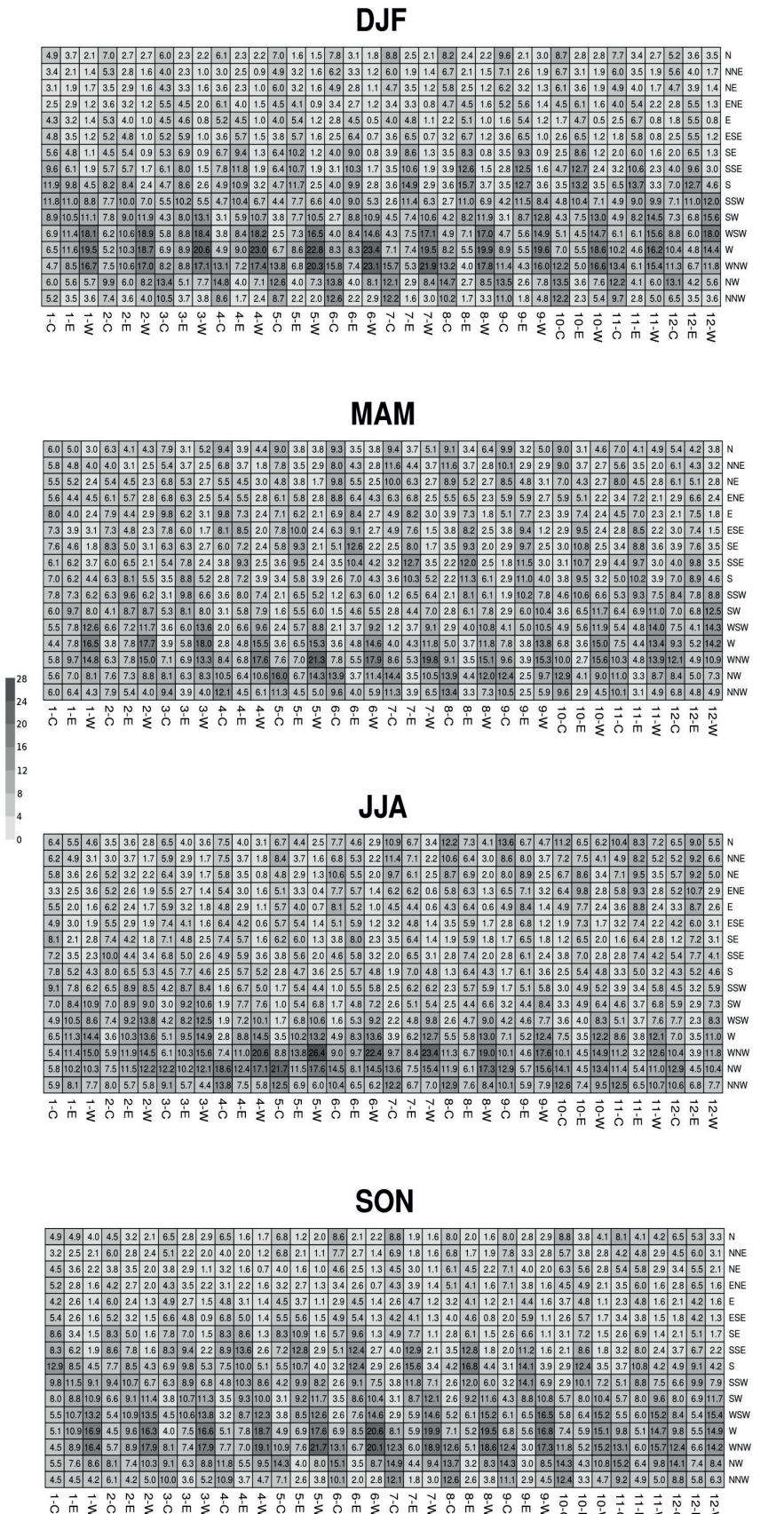


Fig. 7 Seasonal directional structure (%) of geostrophic wind for triangles (1 to 12 – west to east) in VG macro-forms C, E and W, 1981–2015



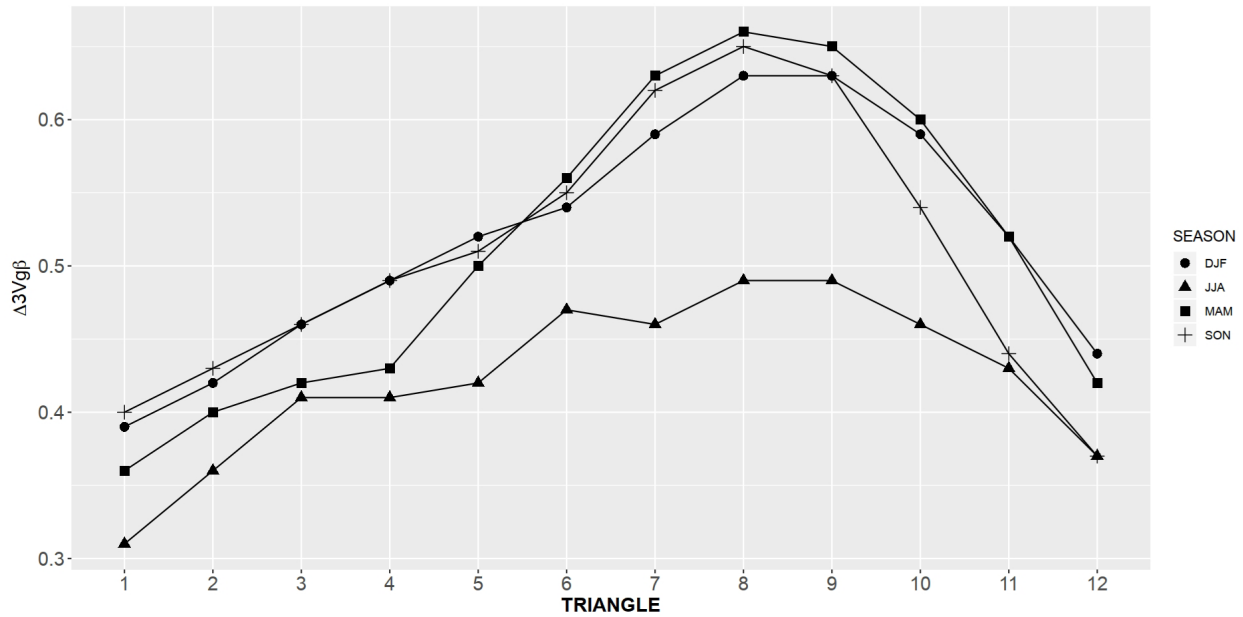


Fig 8. Seasonal values of the index of Vg vectors differences  $\Delta_3V_g\beta$  (Equation 4) at triangles 1 to 12 (west to east), (1981–2015)

Table 5 Seasonal values of the index of directional structure differences  $\Delta_3V_gf$  (Equation 5) for triangles 1 to 12 (west to east) (1981–2015). Three highest seasonal values are bolded.

Triangle/ Season	1	2	3	4	5	6	7	8	9	10	11	12
DJF	0.67	0.67	0.77	0.92	0.91	0.92	<b>0.96</b>	<b>0.98</b>	<b>0.94</b>	0.89	0.78	0.69
MAM	0.55	0.58	0.68	0.70	0.76	0.79	<b>0.83</b>	<b>0.83</b>	<b>0.84</b>	0.81	0.68	0.58
JJA	0.50	0.53	0.61	0.72	<b>0.78</b>	0.71	<b>0.75</b>	<b>0.73</b>	0.70	0.63	0.58	0.57
SON	0.63	0.64	0.68	0.78	0.84	<b>0.92</b>	<b>0.96</b>	<b>0.95</b>	0.91	0.75	0.64	0.61

Table 6. Seasonal values of the index of wind directions differences  $\Delta_3V_g\alpha$  (Equation 3) at triangles 1 to 12 (west to east) (1981–2015). Three highest seasonal values are bolded

Triangle/ Season	1	2	3	4	5	6	7	8	9	10	11	12
DJF	0.43	0.44	0.51	0.54	0.57	0.61	0.71	<b>0.77</b>	<b>0.78</b>	<b>0.77</b>	0.75	0.73
MAM	0.47	0.53	0.65	0.71	0.75	<b>0.83</b>	<b>0.86</b>	<b>0.85</b>	<b>0.83</b>	<b>0.83</b>	0.76	0.67
JJA	0.49	0.58	<b>0.78</b>	<b>0.82</b>	0.74	<b>0.84</b>	<b>0.78</b>	0.74	0.73	0.68	0.70	0.70
SON	0.60	0.62	0.69	0.67	0.64	0.72	<b>0.81</b>	<b>0.87</b>	<b>0.86</b>	<b>0.81</b>	0.76	0.75

## Conclusions and discussion

The presented results clearly indicate that the air flow conditions recorded in the lower troposphere in the 50–60°N zone over Europe remain in direct connection with the mid-troposphere circulation defined by the Vangenheim-Girs macro-forms.

During the period 1981–2015, VG macro-form frequency was close to the 1891–2001 characteristics provided by Seep (2005) when there were 41.5% of days with macro-form *E*, 33.0% (*W*) and 25.5% (*C*). The frequency in the period 1981–2015 “returned” to the multi-annual norm as the preceding 30-year period (1951–1980) exhibited substantially decreased frequencies of macro-form *W* ( $f_d W = 23.3\%$ ) with high frequencies of meridional circulation macro-forms ( $f_d E = 51.1\%$ ,  $f_d C = 25.5\%$ ). In the end of the 1980s the span of dominating zonal circulation began, which was forecasted by Girs (1977).

Macro-form *W* corresponds to the most intense and stable western airflow. Westerlies’ intensity diminishes substantially towards the east of Europe, which is also indicated by the decrease in zonal SLP gradients. Western  $V_g$  directions (SW–NW) during macro-form *W* episodes are characterised by frequency not larger than *ca.* 63%. Taking average annual frequency of macro-form *W* (33.4%) into account it seems that western  $V_g$  directions connected with macro-form *W* occur for barely 20–25% of days in a year. Thus, meridional circulation patterns dominate.

The VG circulation macro-form *E* is associated with the southern advection in the majority of the 50–60°N zone, which refers to the circulation in the eastern part of the mid-troposphere trough. The macro-form *C* in zone 50–60°N is accompanied by north-western and northern circulation, associated with a similar direction of air advection in the eastern part of the mid-troposphere ridge. The varying directions of geostrophic wind in zone 50–60°N during meridional circulation macro-forms *E* and *C* were recorded in the western part of this zone, located in the region of the mid-troposphere troughs/ridges or to the west of those axes.

The velocity of airflow in the lower atmosphere and the stability of wind direction are lowest in periods when VG macro-form *E* dominates. This type

also results in elevated exposure to the influence of seasonal pressure systems from over Asia. Macro-form *C*, on the other hand, favours the formation of blocking high-pressure systems over Western Europe. It can be stated that meridional circulation macro-forms may almost completely eliminate western advection in the 50–60°N zone. The frequency of westerly winds during macro-forms *E* and *C* does not exceed 5%. It is worth underlining that  $V_g$  characteristics associated with macro-form *E* are not simple reversals of characteristics associated with macro-form *C*. Northern advectations (macro-form *C*) are substantially more intense than southern advectations (*E*). Perhaps it was not without reason that Girs himself called macro-form *C* a southerly one, and *E* easterly.

The greatest variability in geostrophic wind characteristics due to the VG macro-forms is revealed in the central and eastern part of the 50–60°N zone – between the southern Baltic Sea and the western border of Russia, i.e. over the area of the opposite directions of airflow induced by the macro-forms *E* and *C*. The variability of  $V_g$  characteristics over Europe clearly correlates with the location and extent of long waves in the mid-troposphere defining VG macro-forms (Fig. 1). In summary, it should be stated that the classification of Vangenheim-Girs circulation macro-forms can be perceived as a useful tool for the climatological description of general circulation characteristics in both the mid- and low troposphere.

In the previous studies on the impact of VG macro-forms on climate elements (including SLP) (Sepp and Jaagus 2002; Sepp 2005; Marsz 2013), the correlations between frequency of VG forms (monthly or seasonal) and climate elements were generally used. In our paper, instead of frequency, so-called episodes/occurrences of VG macro-forms were taken into account together with the corresponding SLP field and resulting geostrophic wind characteristics describing the atmospheric circulation in the lower troposphere. Three subsets of  $V_g$  characteristics were assigned to the occurring circulation macro-forms: *W*, *E* and *C*. The results obtained with the “composite method” differ slightly from the outcomes from the “correlation method” – the isobars (see, e.g., DJF SLP isobars in Fig. 4) do not coincide with the isocorrelates field in Figures 4.1, 4.2 and 4.3 presented by Sepp (2005).

A simple formula based on three differences ( $\Delta_3 V_g$ , see Eq. 3) was utilised to study the combined effect of macro-forms  $W$ ,  $E$  and  $C$  on the  $V_g$  characteristics. Indices derived from those differences allowed the assessment of the variability of the VG macro-forms impact on the directional structure and  $V_g$  in the analysed zone across Europe.

The above mentioned episodes of circulation forms, equivalent to similar synoptic processes (SSP) mentioned by Girs (1971), differ significantly due to the duration of the SSP. Girs assumed them to last 8–12 days, whereas, in 1981, SSP form  $E$  lasted 116 days. The average duration of circulation episodes had been established indicating the *ca.* seven-day variability in the emergence of VG macro-forms. However, the sequence (order of occurrence) of macro-form episodes, as investigated by Kożuchowski and Degirmendžić (2018) has a stochastic character, whereas long-term fluctuations in the frequency of VG macro-forms are more regular (quasicyclic). VG macro-forms' frequencies are unstable, and their variability directly affects the observed climate change on a regional scale. The southern Baltic Sea area is particularly sensitive to the diverse impact of VG macro-forms. The increasing zonal circulation macro-form  $W$  frequencies at the end of the 20th century are attributed to a positive trend in air temperature in 1980–2009 (2.95°C/100 years) in this area, which was twice as fast compared to that of the northern hemisphere (Ferdynus and Marsz 2010). One cannot rule out the influence of the circulation macro-forms on the average temperature of the entire hemisphere. On the other hand, global warming, particularly in the Arctic, as shown by Overlang and Wang (2010), affects macro-circulation patterns such as the Arctic Oscillation. The AO indices are significantly correlated with the VG macro-forms. Warming of the Arctic therefore affects circulation macro-forms. So far, for quite a long time – for nearly 30 years – the relatively high frequency of the zonal form has been maintained.

## Disclosure statement

No potential conflict of interest was reported by the authors.

## Author Contributions

Study design: K.K., M.M.; data collection M.M., K.K.; statistical analysis: M.M., K.K.; result interpretation K.K., M.M.; manuscript preparation M.M., K.K.; literature review: K.K., M.M.

## References

- BARNSTON AG and LIVEZEY RE, 1987, Classification, seasonality and persistence of low-frequency atmospheric circulation patterns. *Monthly Weather Review*, 115: 1083–1126.
- BIELEC-BAKOWSKA Z, 2010, A classification of deep cyclones over Poland (1971–2000). *Physics and Chemistry of the Earth* 35: 491–497.
- DEE DP, UPPALA SM, SIMMONS AJ, BERRISFORD P, POLI P, KOBAYASHI S, ANDRAE U, BALMASEDA MA, BALSAMO G, BAUER P, BECHTOLD P, BELJAARS ACM, VAN DE BERG L, BIDLOT J, BORMANN N, DELSOL C, DRAGANI R, FUENTES M, GEER AJ, HAIMBERGER L, HEALY SB, HERBACH H, HÓLM EV, ISAKSEN I, KÁLLBERG P, KÖHLER M, MATRICARDI M, MCNALLY AP, MONGE-SANZ BM, MORCRETTE JJ, PARK K, PEUBEY C, DE ROSNAY P, TAVOLATO C, THÉPAUT JN and VITART F, 2011, The ERA-Interim reanalysis: configuration and performance of the data assimilation system, *Quarterly Journal of Royal Meteorological Society* 137: 553–597, <https://doi.org/10.1002/qj.828>.
- DEGIRMENDŽIĆ J, KOŻUCHOWSKI K and WIBIG J, 2000, Epoki cyrkulacyjne XX wieku i zmienność typów cyrkulacji atmosferycznej w Polsce. *Przegląd Geofizyczny*, (45)3–4: 221–238.
- DEGIRMENDŽIĆ J, KOŻUCHOWSKI K and ŻMUDZKA E, 2004, Changes of air temperature and precipitation in Poland in the period 1951–2000 and their relationship to atmospheric circulation, *International Journal of Climatology* 24: 291–310.

- DIMITRIEV AA and BELYAZO VA, 2006, Kalendarny katalog atmosferycznych procesów po cirkumpolarnym w obszarze północnej półkuli i ich charakterystyki za okres 1949–2005 r. In: *Kosmos, planetarnaya klimaticheskaya izmenchivost' i atmosfera polarnykh regionov*. Gidrometeoizdat, St. Petersburg.
- FERDYNUS J and MARSZ AA, 2010, Zmiana charakteru pogód na południowo-wschodnim wybrzeżu Bałtyku wraz ze słabnięciem klimatycznych wpływów Atlantyku w okresie regionalnego wzrostu temperatury. In: Kolondowicz L (ed.), *Klimat Polski na tle klimatu Europy*. Bogucki Wydawnictwo Naukowe, 61–74.
- GIRS AA, 1964, O sozdani i edinoi klassifikacii makrosinopticheskikh processov severnogo polushariia. *Meteorol. i Gidrol.* 4: 43–47.
- GIRS AA, 1974, *Makrocirkulacyonnyy metod dolgorochnykh meteorologicheskikh prognozov*. Gidrometeoizdat, Leningrad.
- GIRS AA, 1977, Mnogoletnije preobrazovaniya form atmosferycznej cirkulacii i kolebanija klimata razlichnykh rajonov severnogo polushariia. In: *Klimatologija i sverkhdolgosrochnyj prognoz*. Gidrometeoizdat. Leningrad, 39–46.
- GIRS AA, 1981, K voprosu o formakh atmosferycznej cirkulacii i ikh prognosticheskomykh ispolzovanii. *Trudy AANII*, 374: 4–13.
- HOY A, JAAGUS J, SEPP M and MATSCHULLAT J, 2013, Spatial response of two European atmospheric classifications (data 1901–2000). *Theoretical and Applied Climatology* (112)1–2: 73–88.
- HUTH R, 2001, Disaggregating climatic trends by classification of circulation patterns. *International Journal of Climatology*, 21: 135–153.
- KOŻUCHOWSKI K, 2004, Cyrkulacja atmosferyczna nad Polską i jej wpływ na warunki klimatyczne. In: Kożuchowski K (ed.), *Skala, uwarunkowania i perspektywy współczesnych zmian klimatycznych w Polsce*. Wyd. Biblioteka, Łódź, 69–81.
- KOŻUCHOWSKI K and DEĞIRMENDŽIĆ J, 2018, Zmienność form cyrkulacji środkowo-troposferycznej według klasyfikacji Wangenheima-Girsa i ich relacje z polem ciśnienia na poziomie morza. *Przegląd Geofizyczny*, (63)1–2: 89–122.
- LAMB HH, 1972, British Isles weather types and a register of daily sequence of circulation patterns, 1861–1971. *Geophysical Memoir*, 116, 85L.
- LITYŃSKI J, 1969, Liczbowa klasyfikacja typów cyrkulacji i typów pogody dla Polski. *Prace PIHM*, 97: 3–14.
- MAROSZ M, 2012, Typy cyrkulacji atmosferycznej w środkowej troposferze regionu atlantycko-europejskiego i ich związek z dolnotroposferycznymi charakterystykami przepływu powietrza nad Europą Środkową (1951–2010). In: Bielec-Bąkowska Z, Łupikasza E, Widawski A (eds), *Rola cyrkulacji atmosfery w kształtowaniu klimatu, Prace Wydziału Nauk o Ziemi Uniw. Śląskiego* 74, 333–343.
- MAROSZ M, 2016, Variability of geostrophic airflow over Poland 1951–2014, *Bulletin of Geography. Physical Geography Series* 10: 5–18. DOI: 10.1515/bgeo-2016-0001, June 2016.
- MAROSZ M, 2017, *Wieloletnia charakterystyka przepływu powietrza nad Polska Północną 1951–2015*. Wyd. Katedra Meteorologii i Klimatologii, Uniw. Gdański, Gdańsk.
- MAROSZ M and MIĘTUS M, 2012, Opis lokalnych aspektów cyrkulacji atmosferycznej za pomocą wektora wiatru geostroficznego. In: Bielec-Bąkowska Z, Łupikasza E, Widawski A (eds), *Rola cyrkulacji atmosfery w kształtowaniu klimatu, Prace Wydziału Nauk o Ziemi Uniw. Śląskiego* 74, 89–100.
- MARSZ AA, 2012, Cyrkulacja atmosferyczna w atlantycko-euroazjatyckim sektorze cyrkulacyjnym – schemat uwarunkowań i mechanizm działania. In: Bielec-Bąkowska Z, Łupikasza E, Widawski A (eds), *Rola cyrkulacji atmosfery w kształtowaniu klimatu, Prace Wydziału Nauk o Ziemi Uniw. Śląskiego* 74, 101–117.
- MARSZ AA, 2013, Frekwencja makrotypów cyrkulacji środkowotroposferycznej według klasyfikacji Wangengejma-Girsa a pole ciśnienia atmosferycznego nad Europą i północną Azją. *Przegląd Geofizyczny*, (58)1–2: 3–24.
- MIĘTUS M, 1993, Lokalny wskaźnik cyrkulacji atmosferycznej nad południowym Bałtykiem w odniesieniu do wiatru i temperatury na polskim Wybrzeżu. In: Kożuchowski K (ed.), *Globalne ocieplenie a współczesne zmiany klimatyczne w Polsce. Materiały Międzynarodowej Konferencji, Uniw. Szczeciński 31.05–1.06.1993*: 223–231.
- MIĘTUS M, 1995, Vector of geostrophic wind in the North Atlantic region as an index of local atmospheric sub-circulation. *Proceeding of the 6th International Meeting on Statistical Climatology*, Galway, June 19–23, University College, Ireland: 227–230.
- MIĘTUS M, 1996, Zmienność lokalnej cyrkulacji atmosferycznej nad północną Polską i jej związek z elementami klimatu. *Wiadomości IMGW* (20)1: 9–29.

- NOWOSAD M, 2017, Variability of the zonal circulation index over Central Europe according to the Lityński method. *Geographia Polonica* (90)4: 417–430.
- OVERLAND JE and WANG M, 2010, Large-scale atmospheric circulation changes are associated with the recent loss of Arctic sea ice, *Tellus A: Dynamic Meteorology and Oceanography* (62)1: 1–9, DOI: 10.1111/j.1600-0870.2009.00421.x.
- SEPP M, 2005, Influence of atmospheric circulation on environmental variables in Estonia. *Dissertationes Geographicae Universitatis Tartuensis* 25.
- SEPP M and JAAGUS J, 2002, Frequency of circulation patterns and air temperature variations in Europe. *Boreal Environment Research* (7)3: 273–279.
- SEPP M, POST P and JAAGUS J, 2005, Long-term changes in the frequency of cyclones and their trajectories in central and northern Europe. *Nordic Hydrology* 36: 297–309.
- WASA, 1998, Changing waves and storms in the north-east Atlantic? *Bulletin of American Meteorological Society*, 79: 741–760.
- WIBIG J, 1999a, Cyrkulacja atmosferyczna nad Europą na powierzchni izobarycznej 500 hPa. Część I: Zima. *Przegląd Geofizyczny* (44)1–2: 15–24.
- WIBIG J, 1999b, Cyrkulacja atmosferyczna nad Europą na powierzchni izobarycznej 500 hPa. Część II: Wiosna, lato, jesień. *Przegląd Geofizyczny*, (44)1–2: 25–38.
- WILKS D, 2011, *Statistical Methods in the Atmospheric Sciences*, Academic Press.
- van BEBBER W, 1891, Die Zugstrassen der barometrischen Minima. *Meteorologische Zeitschrift*, 8: 361–366.
- VANGENHEIM GJA, 1946, O kolebaniakh atmosfernoï cirkulacii nad severnym polushariem. *Izvestiia Akademii Nauk SSSR* X, 5: 407–416.
- VANGENHEIM GJA, 1952, Osnovy makrocirkulacionno-go metoda dolgosrochnykh meteorologicheskikh prognozov dlia Arktiki. *Trudy AANII* 34: 11–66.

Received 17 December 2018

Accepted 23 April 2019